Dissociative recombination of the weakly bound NO-dimer cation: Cross sections and three-body dynamics

Annemieke Petrignani[a)]
FOM Institute for Atomic and Molecular Physics, Kruislaan 407, 1098 SJ, Amsterdam, The Netherlands

Patrik U. Andersson and Jan B. C. Pettersson
Department of Chemistry, Atmospheric Science, Göteborg University, SE-412 96 Göteborg, Sweden

Richard D. Thomas, Fredrik Hellberg, Anneli Ehlerding, and Mats Larsson
Department of Physics, Stockholm University, AlbaNova University Centre, SE-106 91 Stockholm, Sweden

Wim J. van der Zande
Institute for Molecules and Materials, Radboud University Nijmegen, Toernooiveld 1, 6525 ED Nijmegen, The Netherlands

(Received 10 May 2005; accepted 19 September 2005; published online 14 November 2005)

Dissociative recombination (DR) of the dimer ion $(NO)_2^+$ has been studied at the heavy-ion storage ring CRYRING at the Manne Siegbahn Laboratory, Stockholm. The experiments were aimed at determining details on the strongly enhanced thermal rate coefficient for the dimer, interpreting the dissociation dynamics of the dimer ion, and studying the degree of similarity to the behavior in the monomer. The DR rate reveals that the very large efficiency of the dimer rate with respect to the monomer is limited to electron energies below 0.2 eV. The fragmentation products reveal that the breakup into the three-body channel NO+O+N dominates with a probability of 0.69±0.02. The second most important channel yields NO+NO fragments with a probability of 0.23±0.03. Furthermore, the dominant three-body breakup yields electronic and vibrational ground-state products, $NO(v=0)+N(^4S)+O(^3P)$, in about 45% of the cases. The internal product-state distribution of the NO fragment shows a similarity with the product-state distribution as predicted by the Franck-Condon overlap between a NO moiety of the dimer ion and a free NO. The dissociation dynamics seem to be independent of the NO internal energy. Finally, the dissociation dynamics reveal a correlation between the kinetic energy of the NO fragment and the degree of conservation of linear momentum between the O and N product atoms. The observations support a mechanism in which the recoil takes place along one of the NO bonds in the dimer. © *2005 American Institute of Physics*. [DOI: 10.1063/1.2116927]

I. INTRODUCTION

Diatomic ions such as O_2^+, NO^+, and N_2^+ are of major importance to the Earth's ionosphere and play an important role in the ionospheric chemistry and heating.[1,2] Cluster ions are of importance in the lower part of the *D* region.[3] Below roughly 85 km, water-cluster ions dominate over O_2^+ and NO^+, and become more important as sinks for low-energy electrons and as a source of reactive and kinetic species. Of special importance to the water-cluster ion formation is the production and loss of O_2^+ and NO^+ dimer ions, where NO^+ clusters with other neutrals rather than with its neutral counterpart due to low NO densities. The dimer ions are weakly bound and experiments suggest that their thermal dissociative recombination (DR) rate coefficients are an order of magnitude faster than their monomer counterparts.[4] This large recombination rate is referred to as super-DR and is not restricted to weakly bound dimer ions, but hold for strongly bound (proton-bridged) and rare-gas dimer ions as well.[5,6] As far as we know, neither branching nor collision-energy-dependent rate coefficients have been determined for weakly bound dimer ions. Although $(NO)_2^+$ has no direct importance to the Earth's atmosphere, its study can provide insight on the behavior of the rate and on the influence of this bond type on the DR reaction.

The NO-dimer cation has been characterized experimentally using various spectroscopic methods such as matrix spectroscopy[7,8] and more recently using zero electron kinetic energy (ZEKE) spectroscopy.[9] This ion has posed theoreticians many problems both in explaining the spectroscopic results as well as in establishing the theoretical tools for predicting the correct binding properties.[9–11] The *trans* (ON–NO) configuration is the minimum-energy configuration; the *cis* (ONNO) configuration is nearly isoenergetic. A *cyclic* (.ONON.) structure is positioned about 0.2 eV above the ground state.[12] This cyclic configuration is invoked in explaining some vibrational frequencies observed using matrix spectroscopy. The N–N bond strength that binds the NO moieties has been determined to be around 0.6 eV.[13–15] The vibrational frequency of the NO moiety in the dimer ion is larger than that of NO and smaller than that of NO^+, indicating that in the dimer ion the effective charge is 0.5 on each NO moiety.[13] The N–N equilibrium distance in the dimer

a)Electronic mail: annemieke@petrignani.nl

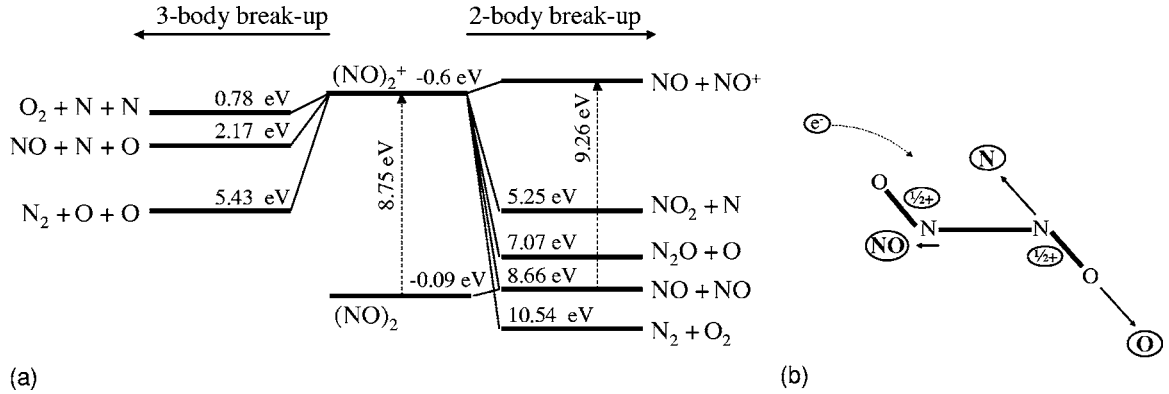

FIG. 1. (a) Level diagram concerning the DR of the NO-dimer cation. The three-body breakup is displayed on the left and the two-body breakup on the right. The dashed vertical arrows denote the ionization energy of the dimer and monomer molecule. The two negative values are the binding energies of the dimer neutral and ion. (b) Geometric structure of the *trans* isomer of $(NO)_2^+$. The circled labels are the particles involved in the DR reaction branching towards the NO+O+N channel. The positive charge in the parent ion is equally divided over the NO moieties. The solid arrows illustrate the momentum vectors of the product fragments when no rearrangements occur upon dissociation into NO+O+N.

ions is calculated to be 2.22 Å (*cis*) and 2.24 Å (*trans*), illustrative of the relatively weak bond.[10] Although we do not have explicit information on the configurations from our ion source, we believe that the dimer ions are predominantly produced in the *cis* and *trans* configurations.

At 0 eV collision energy, E_c, and for electronic and vibrational ground-state ions, the DR of $(NO)_2^+$ may result in the following chemical fragmentation processes and corresponding kinetic-energy releases (KERs):

$$(NO)_2^+ + e^-(E_c = 0) \rightarrow N_2 + O_2 + 10.54 \text{ eV} \quad (1a)$$

$$\rightarrow NO + NO + 8.66 \text{ eV} \quad (1b)$$

$$\rightarrow N_2O + O + 7.07 \text{ eV} \quad (1c)$$

$$\rightarrow N_2 + O + O + 5.43 \text{ eV} \quad (1d)$$

$$\rightarrow NO_2 + N + 5.25 \text{ eV} \quad (1e)$$

$$\rightarrow NO + O + N + 2.17 \text{ eV} \quad (1f)$$

$$\rightarrow O_2 + N + N + 0.78 \text{ eV}. \quad (1g)$$

The KER values given in Eqs. (1a)–(1g) are valid when all product fragments are created in their electronic and vibrational ground states. Internal excitation of the fragments increases the number of dissociation pathways. Equation (1f) would, for example, split into the following "physical" branching channels:

$$(NO)_2^+ + e^-(E_c = 0)$$

$$\rightarrow NO + O(^3P) + N(^4S) + 2.17 \text{ eV} \quad (2a)$$

$$\rightarrow NO + O^*(^1D) + N(^4S) + 0.21 \text{ eV} \quad (2b)$$

$$\rightarrow NO^*(v,J) + O(^3P) + N(^4S) + (2.17 - E_{v,J}) \text{ eV} \quad (2c)$$

$$\rightarrow NO + O(^3P) + N^*(^2D) - 0.21 \text{ eV}. \quad (2d)$$

The stars indicate the internal excitation of the specific fragment. The KER values given in Eqs. (2a), (2b), and (2d) are valid for 0-eV collisions and for the parent ion as well as the NO product fragment in their rovibrational ground state. Equation (2c) groups together a number of energetically possible channels, expressed as $NO^*(v,J)$, where $E_{v,J}$ is the excitation energy of the respective states with respect to the rovibronic ground state of NO. Equation (2d) is not energetically possible at 0-eV collisions unless aided by 0.21 eV of internal excitation in the $(NO)_2^+$ parent ion. We note that this energetically inaccessible dissociation towards $O(^3P) + N^*(^2D)$ is, in fact, the dominant dissociation pathway in the DR of the monomer NO^+. We also note that dissociation towards $O^*(^1D) + N(^4S)$, which is energetically and spin allowed in the dimer ion, is not observed in the DR of the monomer ion in accord with the conservation of electron spin during the DR reaction.[16]

Figure 1(a) summarizes the reactions (1a)–(1g). The three-body-reaction channels are given on the left-hand side and the two-body-reaction channels on the right-hand side. The binding energy of the neutral dimer (0.09 eV) is much smaller than that of the ionized dimer (0.6 eV). Figure 1(b) shows the geometry associated with the ground-state *trans* configuration of the NO-dimer ion. For illustration purposes, the outcome of a dissociation process involving recoil along one of the NO bonds is indicated; the result being energetic O and N fragments and a smaller kinetic energy of the NO product.

The present research aims at investigating the underlying mechanisms responsible for the enhanced thermal DR rates for dimer ions and studies the degree of similarity between the DR of $(NO)_2^+$ and the DR of its monomer. We present data on the energy dependence in the efficiency of the DR process as well as new data on the chemical branching, identifying the product fragments, and on the physical branching, qualitatively identifying the internal state and the kinetic energy of the nascent products. In addition, the energy-dependent cross section of the dissociative excitation (DE) of

$(NO)_2^+$ into $NO+NO^+$ is presented as well. The results from the DR study are compared with those found for other weakly and strongly bound dimer ions.

II. EXPERIMENT

The present studies have been carried out at the heavy-ion storage ring CRYRING at the Manne Siegbahn Laboratory, Stockholm. The experimental procedures for measuring cross sections, chemical fragmentation,[17,18] and physical fragmentation[16] have been presented in detail in literature and are therefore only briefly described here. The $(NO)_2^+$ ions were produced from pure NO vapor in a high-pressure hollow cathode ion source (JIMIS).[19] An ion current of about 0.5 nA was obtained and stored. After extraction from the source, the $(NO)_2^+$ ions were mass selected and injected into the ring at a platform energy of 40 keV, where they were further accelerated to the maximum energy of 1.6 MeV in about 1 s. The ions were then allowed to coast in the ring for 8 s. In one of the straight sections of the ring, the so-called electron cooler, an electron beam was merged with the ion beam for ion-electron reactions to occur. The electron cooler has a length of 0.85 m and the total circumference of the storage ring is 51.6 m. The ion beam passes the electron beam many times during its storage. The relevant reactions occurring in the electron cooler are the DR and, if energetically possible, the DE reactions. The DE of $(NO)_2^+$ into $NO+NO^+$ is the first DE channel that becomes energetically possible and this reaction requires an additional energy of 0.6 eV [see Fig. 1(a)]. Reactions such as resonant ion-pair formation[20] and dissociative ionization[19] may also occur when additional energy is available; however, these reactions produce only charged fragments. Superelastic collisions may occur at all times and internally relax the ions.[21] The DR reaction produces only neutral fragments, while the DE reaction produces both neutral and positively charged fragments. Collisions between the ions and rest-gas molecules occur throughout the ring and, just as for DR and DE, produce (partly) neutral product fragments. The collisions occurring in the entire straight section enclosing the electron cooler give rise to a background signal in the DR and DE studies. The neutral product fragments from any of the reactions in the straight section are unaffected by the dipole magnet and will continue in a straight line towards a zero-degree arm containing our detection systems, while the remaining ions continue to coast inside the ring. The detection techniques used are described below. It is noted that in the two outermost regions of the electron cooler, the electron beam is not parallel to the ion beam due to the merging and demerging processes. These so-called toroidal regions have to be accounted for. The toroidal correction has been included both in the data analysis and in the parametrization of the dissociation dynamics.[16,22] The electron space-charge effect, which is due to the trapping of positive ions in the space charge of the electron beam, has also been taken into account to extract the energy-dependent cross sections.[23]

A. Cross-section measurements

For cross-section measurements, an energy-sensitive silicon semiconductor detector, a so-called surface barrier detector (SBD), is used to measure the count rate of the reaction of interest. The SBD used was mounted at a distance of ca. 4 m from the center of the electron cooler and has an active area with a diameter of 34 mm. At MeV energies, the SBD gives an output signal that is proportional to the kinetic energy of the incoming neutral fragments. It cannot detect the fragments per dissociation event separately; the time-of-arrival difference of a few nanoseconds between the fragments at MeV energy is shorter than the detector's integration time. DR events therefore always give rise to an output-signal height that is characteristic of the full beam energy.

Thus in studying the DR cross section, the count rate of signals corresponding to the total beam energy is measured. In the case of $(NO)_2^+$ this means that the rate of events with a total mass of 60 amu is measured. In studying the DE cross section of $(NO)_2^+$ into $NO+NO^+$, the count rate of signals corresponding to half the total beam energy, i.e., the rate of events with a total mass of 30 amu, is measured. Background collisions may give rise to signals of both half and total beam energies.[24] These contributions can be determined whenever the DR or the DE signal is absent.

The DR and DE signals have been measured while ramping the collision energy between 0–1 and 0–4 eV, respectively. Both measurements used acceleration and deceleration of the electrons to ensure that a collision energy of 0 eV is achieved. It is noted that for heavy ions like the present ion, the experiment at CRYRING has to employ low-energy electron beams. The electron gun cathode was set to a mere 16 eV in order to attain 0 eV collision energy and during the ramps it varied between 9–25 and 9–36 eV for the DR and DE measurements, respectively. From injection until the starts of the measurements the electrons were set to a nominal 0 eV collision energy to ensure cooling (the energy resolution is 2 meV near 0 eV and worsens at higher collision energies). The measurements were started after 5 s storage time and lasted for 1.5 s. The background contribution was determined with the electron beam turned off in the DR measurement and through the mass-30 signal at collision energies below the DE threshold energy in the DE measurement.

B. Chemical branching at 0 eV

To measure the chemical fragmentation for the different channels of the DR process [see Eqs. (1a)–(1g)], a metal grid with a transmission $T=0.297\pm0.015$ was inserted in front of the SBD.[17] This grid is thick enough to stop any of the neutral fragments that do not pass through the holes. Thus the probability for a neutral fragment to pass through the grid is T, and the probability for the fragment to be stopped is $(1-T)$. Since each neutral fragment carries a fraction of the total beam energy proportional to its mass and may pass while other fragment(s) are stopped, the total DR signal is split into a series of peaks corresponding to beam-energy fractions determined by mass ratios. For example, the product channel NO+NO has a chance of T^2 for both products to

pass, resulting in a peak at full energy weighed by this probability. There is also twice the chance that one NO will pass while the other NO is stopped, i.e., $2T(1-T)$, both resulting in a peak at half beam energy weighed by their respective probability. Each product channel can be treated similarly, resulting in a set of linear equations that relate the number of counts in the different energy-fraction peaks to the fragmentation number in the different product channels,

$$\mathbf{I} = \mathbf{MF},$$

where **I** is the vector containing the eight background-corrected intensities of the energy-fraction peaks related to the transmitted fragment masses 60 (2N+2O), 46 (N+2O), 44 (2N+O), 32 (2O), 30 (N+O), 28 (2N), 16 (O), and 14 (N); **F** is the vector containing the seven branching intensities, F_{1i}, with $i=a-g$ referring to Eqs. (1a)–(1g); and **M** is an 8×7 matrix containing products of $T^n(1-T)^m$, as described above. The branching fractions are obtained after normalization of the branching intensities to the total number of dissociations recorded.

We measured the $(NO)_2^+$ fragment-energy spectra at 5–8 s after injection, while keeping the collision energy at a nominal 0 eV. The background contribution was determined with the electron beam turned off.

C. Physical branching at 0 eV

To measure the physical fragmentation of the DR process, the SBD was removed so that the neutral fragments could reach the imaging system further down the zero-degree arm. The imaging detection system consisted of three microchannel plates and a phosphor plate, located 6.3 m from the center of the electron cooler, followed by an optical system and a charge-coupled device (CCD) camera. This detection system was set up identical to the dynamics study in the DR of diatomic ions.[16] For each event, the positions of all hits on the detector were recorded, irrespective of the number of particles. The identities and the difference in the time of arrival of the particles were not measured. Particle identification has been employed for measurements of the three-body breakup in polyatomic ions where two of the product fragments are considerably lighter than the heavier fragment.[25] We measured the $(NO)_2^+$-imaging spectra at 5–7 s after injection, while keeping the collision energy at a nominal 0 eV. In the data analysis, we focused on all recorded three-particle events. We note that four particles are also recorded. As four-body fragmentation is highly unlikely in our experiment, we attribute the fourth spurious particle to noise interpreted as a particle in the detection scheme. The ratio of three-to-four particle events was about 20 to 1. We therefore estimate that a maximum of 5% of the observed three-particle events may be the consequence of similar events with two recorded particles and a noise hit. We did not investigate the two-particle events; this sample contains many three-particle events in which one fragment remains undetected. As the detectors do not have a 100% detection efficiency, the two-body channel analysis is impossible at present. Finally, the background contribution from the rest-gas collisions was determined with the electron beam turned off.

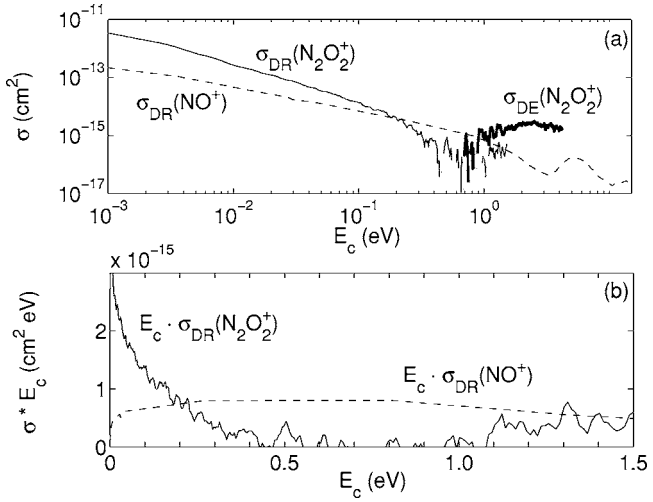

FIG. 2. (a) The DR and DE cross sections of $(NO)_2^+$ together with the DR cross section of NO^+ measured by Vejby-Christensen *et al.* (Ref. 26). The DR cross section of the dimer shows a steeper decrease upon increasing collision energy than that of the monomer. This results in the DR cross section of the dimer becoming comparable to that of the monomer around 0.2 eV. The DE cross section of the dimer is observable as soon as the energy is high enough for the N–N bond to break. The DE rate is comparable to the DR rate at the same energies. (b) The reduced DR cross section, $E_c\sigma_{DR}$, of $(NO)_2^+$ and NO^+/. Note that both axes are on a linear scale. The cross section of the monomer shows an energy dependence that is roughly $1/E_c$, whereas that of the dimer shows a much faster decrease upon increasing collision energy.

III. RESULTS

In the following we will first present the cross-section determinations involving DR and DE of the NO-dimer ion, followed by the chemical and then the physical branching.

A. Absolute DR and DE cross sections

The DR cross section has been measured for collision energies up to 1.4 eV and is shown in Fig. 2(a) together with the DR cross section of the NO^+ monomer.[26] The absolute $(NO)_2^+$ cross section is almost 10^{-11} cm^2 near 1 meV, which is indeed large compared to the value for the monomer ion. However, the cross sections of the dimer and the monomer are comparable near 0.2 eV. Apparently the unusually large DR rate is limited to collision energies below 200 meV. The enhanced DR rate at very small energies suffices to arrive at a high thermal rate. Using the data in Fig. 2(a), we derive a thermal rate of 1.5×10^{-6} cm^3 s^{-1} at 300 K, which is indeed a factor of 4 higher than the thermal rate of the monomer. Since the threshold behavior of DR predicts a cross section $(\langle\sigma v\rangle/v$, with $\langle\ \rangle$ the averaging over the relative velocity distribution) scaling as $1/E_c$ at low collision energies, we also present the data in the form of a reduced cross section, which is the energy-dependent cross section multiplied with the collision energy. Figure 2(b) shows this reduced DR cross section on a linear scale, both in energy and in reduced cross section. A constant value would imply a $1/E_c$ behavior of the cross section. However, as can be observed, the energy de-

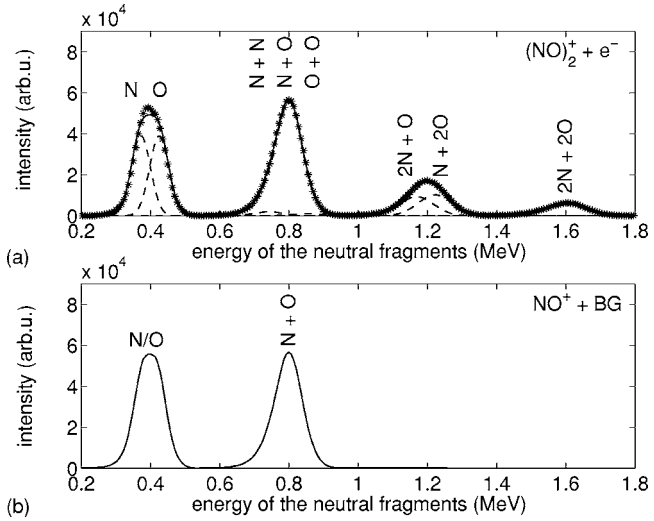

FIG. 3. (a) The energy spectrum of neutral fragments formed in the DR of $(NO)_2^+$ detected with a grid in front of the surface barrier detector. The experimental data (∗), the total fit to the experimental data (solid curve), and the transmitted fragment compositions resulting in the different peaks (dashed curves) are indicated. (b) The energy spectrum observed when NO^+/ was stored in the ring at the same beam energy per amu, as used in the $(NO)_2^+$-cluster experiment.

pendence in the cross section of the dimer is much steeper than $1/E_c$. After accounting for the 2 meV collision-energy resolution in our experiment, the dependence is determined to be $\sigma_{DR} \sim E_c^{-1.4}$. In Fig. 2(b), the beginning of an increase around 1 eV can be observed, which may be related to a secondary maximum in the cross section. Figure 2(a) shows that at this maximum the cross section approaches values that are again consistent with the $\sigma \sim E_c^{-1.4}$ behavior, whereas the intermediate values have a lower cross section. This behavior is similar to that observed in the DR cross section of the NO monomer [see Fig. 2(a)], where a secondary maximum is observed around 5 eV. Finally, Fig. 2(a) also shows the DE cross section of $ONNO^+ \rightarrow NO^+ + NO$. The DE signal is observed as soon as the collision energy is high enough to break the N–N bond (0.6 eV). The DE curve is consistent with the fact that the $(NO)_2^+$ is not hot or contains metastable isomers with small binding energies. The intensity and the trend of the DE cross section are comparable to that of the DR cross section at the same energies. In fact, the NO monomer and the NO dimer share a feature which may be coincidental. In the monomer, one finds an increase in the DR rate around 13 eV, where also the DE rate has its first onset (see Fig. 6 in Ref. 26). The increase for the dimer ion below 1 eV also coincides with the onset of the DE signal, in accord with the idea that both DE and DR often proceed through the same capture states.

B. Chemical fragmentation of the NO-dimer cation

The measured fragment-energy spectrum of the DR signal at 0-eV collisions is shown in Fig. 3(a). The background contribution was measured with the electrons turned off and subtracted from the total signal after normalization. The DR spectrum shows four broad peaks containing DR events, of which 1, 2, 3, or 4 of the atoms passed through the grid. These broad peaks actually consist of more than one mass contribution. For example, the first peak corresponds to a combination of masses 14 (N) and 16 (O), respectively, while the second peak corresponds to some fragment combination of masses 28 (N_2 or N+N), 30 (NO or N+O), and 32 (O_2 or O+O). A separate experiment was carried out where NO^+ was stored in the ring at the same kinetic energy per amu, as used in the $(NO)_2^+$ experiment. The purpose of this experiment was to determine the shape and width of the peak resulting from mass-30 fragments to determine its contribution in the $(NO)_2^+$ energy spectrum. The observed NO^+ energy distribution is shown in Fig. 3(b), where the second peak corresponds to mass 30 only. A detailed comparison between the spectra in Figs. 3(a) and 3(b) shows that the second peak in Fig. 3(a) can almost fully (to 95%) be explained by a combination of NO and N+O fragments. This indicates that the fragment contribution of masses 28 and 32 (N_2, N+N, O_2, and O+O) to the second peak is small, and the branching fractions for Eqs. (1a), (1d), and (1g) are low. The energy spectrum shown in Fig. 3(a) was fitted with a set of model distributions for the different masses. The model distributions for masses 28, 30, and 32 were assumed to have the same shape and width as observed for NO in Fig. 3(b). The contributions of the other masses were described by Gaussian distributions with the width treated as a fitting parameter and the restriction that the overlapping Gaussians have equal widths.

TABLE I. The chemical branching fractions for the DR of $(NO)_2^+$ at a collision energy of 0 eV. The values are given with 95% confidence intervals.

Channel	Product fragments	Chemical branching fraction
1a	N_2+O_2	0.00±0.04
1b	NO+NO	0.23±0.02
1c	N_2O+O	0.00±0.04
1d	N_2+O+O	0.02±0.03
1e	NO_2+N	0.03±0.01
1f	NO+O+N	0.69±0.01
1g	O_2+N+N	0.03±0.02

The number of counts in each mass contribution is used to determine the chemical branching fractions (see Sec. II B). The results obtained after solving the matrix equation and after normalization are summarized in Table I. The three-body breakup into NO+O+N dominates the chemical fragmentation with 69%. The two-body breakup into NO+NO is the second largest fragmentation channel. The other fragmentation channels are small or not significantly present.

C. Physical fragmentation of the NO-dimer cation

Using the fragment imaging system, we analyzed only the three-particle events, which are dominated by the NO +O+N channel, complemented with a small probability of N_2+O+O, O_2+N+N, and a small fraction of false events (see Sec. II C). All three-particle events, after background subtraction from rest-gas collisions, were assumed to come from NO+O+N dissociations. For each event the fragment positions were recorded, which determine two of the three

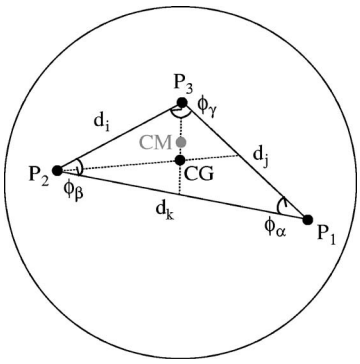

FIG. 4. An example of the positions of the hits on the imaging detector in a three-particle event is shown together with the imaginary triangle that can be drawn through these coordinates. The hits, labeled P_1, P_2, and P_3, do not identify the fragments. The center of geometry (CG) is therefore calculated instead of the center of mass (c.m.). The positions of the particles in the CG frame relate to the kinetic-energy fraction of each fragment. In the analysis of all three-particle events, the following parameters are calculated and investigated: the CG, the three projected interfragment distances (d_i, d_j, and d_k), and the three projected interfragment angles (ϕ_α, ϕ_β, and ϕ_γ). All parameters are sorted by size per event in order to investigate the parameters and their ratios on an event-by-event basis.

components of the fragment velocities originating from the kinetic energy released in the reaction. Each event on our detector provides the parameters shown in Fig. 4. The microchannel plate detector cannot establish the fragment identities. The center of mass (c.m.) is therefore undetermined and we use the center of geometry (CG) instead. As we record projected values, we cannot deduce the physical branching for each event but have to draw conclusions based on the observed distributions. For an unambiguous determination of the physical branching the KER associated with each event has to be known. To this end, the so-called total displacement (TD) is determined, which relates the observed positions and interfragment distances on the detector to the total "projected" KER per event. TD distributions are used to extract the branching fractions. For the DR of $(NO)_2^+$ the TD is expressed as

$$\mathrm{TD} = \sqrt{2(d_{\mathrm{CG}-P_s}^2 M_{\mathrm{NO}}/M_{15} + d_{\mathrm{CG}-P_m}^2 + d_{\mathrm{CG}-P_l}^2)}. \tag{3}$$

Here, M_{NO} and M_{15} stand for the masses of NO and O/N, respectively. The distances, $d_{\mathrm{CG}-P_s}$, $d_{\mathrm{CG}-P_m}$, and $d_{\mathrm{CG}-P_l}$ indicate the shortest, intermediate, and longest distances from the CG, respectively. The TD converges to an interfragment distance as in a diatomic dissociation when the particle P_s receives no kinetic energy.[27] As can be seen, the determination of the TD values does require an identification of the fragments. The TD is therefore based on the assumption that the NO fragment is closest to the CG, whereas the remaining fragments were assumed to be identical fragments of mass 15 instead of 16 (O) and 14 (N). We can check the consequence of the incorrect identifications of fragments in the data analysis with the Monte Carlo simulations.

1. Analysis of the dissociation dynamics

In the following, we present our observations through the parameters illustrated in Fig. 4. In the next section, the observed spectra are recreated with a parametrization of the dissociation process. Figures 5(a)–5(d) show the parameter distributions using the measured events. Figure 5(a) shows the TD distribution, as determined with Eq. (3). For refer-

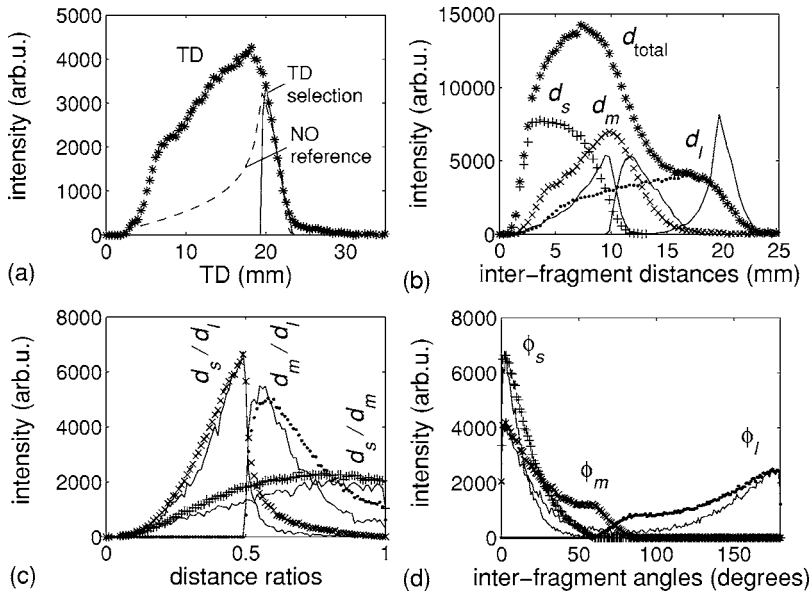

FIG. 5. The parameter distributions as determined from the measured data. (a) The TD distribution (∗) together with a reference spectrum of NO^+-monomer ions dissociating with a KER of 2.17 eV (dashed curve) similar to the ground-state dissociation of the dimer ion [see Eq. (2a)]. The TD distribution is based on the assumption that the NO fragment is nearest to the CG. The TD selection (solid curve) corresponds to events of NO(v=0) dissociating near parallel to the detector plane. (b) The total interfragment distance distribution (∗) and its underlying distributions, where for each event the distances, d_i with $i=s$, m, and l, are sorted on smallest (+), intermediate (×), and longest (·) distances, respectively. The solid curves are the sorted distance distributions associated with events from the TD selection and are scaled by a factor of 3. (c) The distributions of the ratios between the sorted distances, d_s/d_m (+), d_m/d_l (·), and d_s/d_l (×). The ratios are defined to range between 0 and 1. The solid curves are the sorted distance ratios associated with events from the TD selection and are scaled by a factor of 6. (d) The angular distributions sorted by size, ϕ_s (+), ϕ_m (×), and ϕ_l (·) for each event. The solid curves are the sorted angular distributions associated with events from the TD selection and are scaled by a factor of 5.

ence purposes, an example distance distribution of a dissociating NO monomer is included, assuming similar storage-ring conditions (beam velocity and travel distance) and a KER value of 2.17 eV. If the NO fragment from the dimer ion would receive neither kinetic nor internal energy, the TD distribution of the NO+O+N limit would be exactly this distribution [see Eqs. (2a) and (3)]. Our TD distribution is clearly different with many more events at small TD values. However, the agreement of the position of the NO-monomer distribution with the shoulder of the TD distribution must be noted. Apparently, upon the DR of the dimer ion, the available energy is released preferentially in kinetic energy. We will first deduce the shape of the TD distribution for a single KER value and then we will reproduce the broad TD distribution using internal excitation of the NO fragment. Figure 5(b) shows all the observed interfragment distance distributions derived from the three-particle events (as shown in Fig. 4). The total distribution is shown together with the underlying distributions with the three distances sorted on length for each event. The long-distance (d_l) distribution extends to large distances. The maxima in the short- (d_s) and the intermediate- (d_m) distance distributions are relatively close. Figure 5(c) shows the ratios between these interfragment distances determined on an event-by-event basis. Both the d_m/d_l and d_s/d_l distributions show a strong maximum at 0.5; the largest distance is often twice as large as the smaller ones. The above observations are consistent with NO receiving a small fraction of the KER while remaining in the middle. Figure 5(c) shows a broad d_s/d_m distribution with a weak maximum around 0.87. The maximum agrees with a conservation of linear momentum between the oxygen and nitrogen atoms. The breadth of this distribution suggests that the dissociation mechanisms often result in a disproportionate kinetic-energy distribution over the O and N atoms, as a consequence of the presence of the NO fragment. Figure 5(d) shows the distributions over the observed interfragment angles in the detection plane (as shown in Fig. 4). Again, the angles are sorted by size for each event. The angular distributions show a preference for the large ϕ_l angles near 180° and a preference for the intermediate ϕ_m and small ϕ_s angles near 0°. Also this is consistent with a dissociation model in which one fragment, probably the NO fragment, is closest to the CG, receiving little kinetic energy in the dissociation process.

In Fig. 5 we discussed all events. We will now check the first impressions on the dissociation process derived from these data by selecting events with specific TD values. Events with TD values larger than 19 mm comprise events with large KER values that dissociate near parallel to the detector plane. Selecting only these events produces the parameter distributions that are displayed as solid curves in Fig. 5. Note, that the d_l-distance distribution no longer has an overlap with the smaller distances, further supporting near-linear dissociation with the heavier NO in the middle. The angular distributions peak even more at very small or 180° interfragment angles. A next step was to divide the TD distribution in slices with different TD values to investigate the contribution of internally excited states. For each slice with a smaller TD value, a contribution of events with smaller KER values is added. The TD division showed that upon decreasing the TD, all d_s, d_m, and d_l distances decrease approximately proportionally and the associated distance-ratio and angular distributions remained relatively the same. Apparently, the dissociation dynamics leading to vibrationally excited NO fragments are similar to the dynamics leading to the ground state.

2. Parametrization of the dissociation dynamics

In the following we present the parametrization of the dissociation dynamics using a Monte Carlo simulation procedure. The aim was to minimize the differences between simulated and observed data with a minimum set of free parameters. This parametrization is not a dissociation model in the sense that intramolecular properties of the potential-energy surfaces of the dimer are invoked. The procedure is very similar to the one used for imaging studies on XH_2^+ ions in Stockholm.[28,29] The simulation introduces the storage-ring experiment taking the length of the interaction region, travel distance, beam velocity, and the toroidal effect into account. In a Monte Carlo procedure dissociations are generated and distributed randomly over the interaction region with random orientations with respect to the beam axis. For each realization, the total kinetic energy available, ε, is an input. The first free parameter is the angle, χ, formed by the asymptotic momenta of the O and N fragments with respect to the c.m. The smaller this angle, the larger the recoil of the heavy NO fragment. The second parameter divides the remaining kinetic energy over the two light fragments and is specified by the parameter ρ, which is defined as $\rho=v_2^2/v_1^2$, such that $0 \leqslant \rho \leqslant 1$ with v_1 and v_2 the velocity vectors of the two light O and N atoms. These atoms were treated as identical particles of mass 15. Using distributions over the two free parameters, χ and ρ, the positions of the fragments on the detector were calculated for each event (see Fig. 4). The simulation procedure allows a direct comparison with the observed spectra as the Monte Carlo procedure does take into account the misidentification of fragments. For example, the simulated TD distribution was determined based on the assumption that the NO fragment is the one closest to the CG. This proved to be the case in 80%–95% of all events in our dissociation parametrization.

The selection comprising of events with the largest TD values (>19 mm), as shown in Fig. 5 (solid curves), was parametrized first. Subsequently, dissociation events giving internally excited NO product states were included, taking the observation into account that the dissociation dynamics leading to excited NO fragments are very similar to that leading to the ground state. The total kinetic energy in the simulation was decreased in steps of 250 meV, which is approximately the vibrational spacing in the NO moiety. This simulated the production of NO fragments with internal energy. Figure 6 shows how in our best simulation all experimental data are reproduced. The presented simulation includes events ranging from maximum kinetic energy and no internal energy to no kinetic energy and maximum internal energy. For illustration, we show the contribution of NO(v

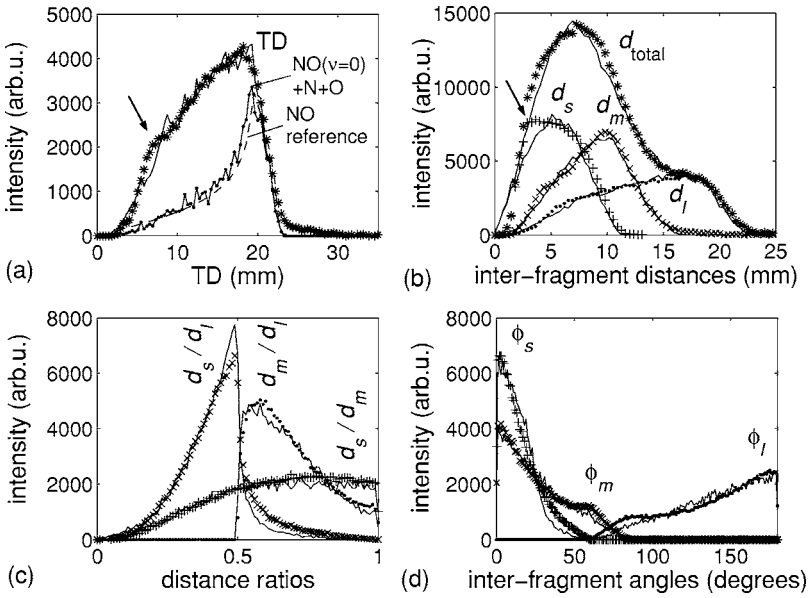

FIG. 6. The simulation (solid curves) that best fitted the measured data (stars). (a) The TD distributions together with the simulated contribution from the NO(v=0)+O+N fragmentation limit [see Eq. (2a)] and a reference spectrum of NO^+-monomer ions dissociating with 2.17 eV kinetic-energy release. The arrow points at a possible indication of the opening of the NO(v=0)+$O^*(^1D)$+N limit [see Eq. (2b)]. (b) The total and underlying *s*-, *m*-, and *l*-distance distributions. The arrow points at the d_s signal associated with the bump observed in the measured TD distribution. (c) The sorted distance ratios d_s/d_m, d_m/d_l, and d_s/d_l distributions. (d) The sorted ϕ_s, ϕ_m, and ϕ_l angular distributions.

=0)+N+O. Note that the distribution is strikingly identical to the reference NO-monomer distribution, which stands for two-particle dissociation dynamics.

The simulation reproducing optimally all observations resulted in the following conclusions. The dissociation dynamics does not depend on the NO internal energy. Furthermore, the angle, χ, peaks near 180°. To get a feeling for the convoluting effect of our detector, Fig. 7 shows the cosine distribution of χ together with that of the associated largest interfragment angles on the detector, ϕ_l. Additionally, we found it necessary to correlate the distribution of $\cos(\chi)$ with that of ρ. When χ is close to 180°, ρ=1. At smaller values of ρ, we allow for a broader range in values of $\cos(\chi)$. For example, a flat distribution in $\cos(\chi)$ for χ=130°–180° seems best in the case of ρ=0.3. To summarize, we conclude that our data set is well described with dissociation events with the following properties. In linear dissociation events, conservation of linear momentum between O and N is observed, as if the NO is a spectator. With increasing kinetic energy of the NO fragments (smaller values of χ), the momenta of the O and N fragments are no longer correlated. It is tempting to conclude that the enhanced kinetic energy of the NO fragments is partially due to intramolecular elastic scattering process of one of the O/N fragments leaving initially with rather high recoil. Our findings agree with a picture in which the dissociation dynamics starts within one of the NO monomers.

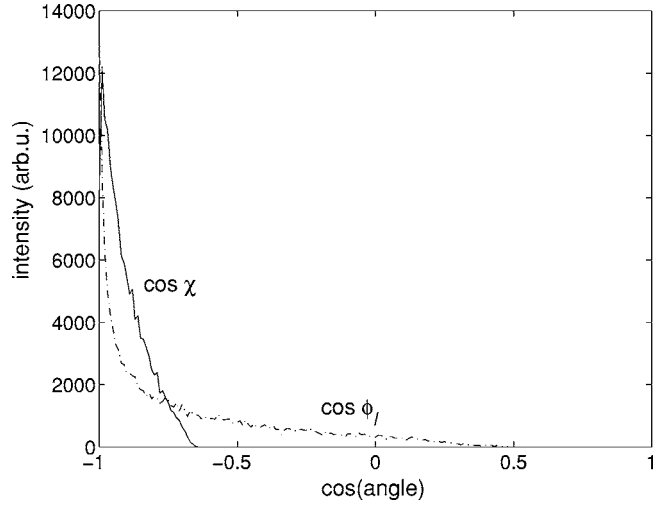

FIG. 7. The total $\cos(\chi)$ (solid curve) and associated $\cos(\phi_l)$ (dashed curve) distributions as used in the simulation shown in Fig. 6. The ϕ_l angles are the $\angle$(O–NO–N) angles as would be measured on the detector, assuming NO is closest to the CG. The χ angles are between 130° and 180° and the ϕ_l angles are between 60° and 180°.

Two questions are of interest at this point. First, do the derived dissociation dynamics imply large or small momentum correlations between the fragments? To answer this, we plot the parametrized dissociation behavior in a so-called Dalitz plot,[30] which has been used in various DR dissociation studies lately.[31,32] This plot makes optimal use of the consequences of the momentum and energy conservation laws in the case of three-particle fragmentation. For a fixed KER, the dissociating systems can be described using only two coordinates, which are linear combinations of the energies of the fragments. These Dalitz coordinates are as follows:

$$Q_1 = \frac{\sqrt{M/m_{\mathrm{NO}}}(E_2 - E_1)}{3\mathrm{KER}}, \tag{4a}$$

$$Q_2 = \frac{(1 + m_{\mathrm{NO}}/m_{15})E_{\mathrm{NO}} - E_2 - E_1}{3\mathrm{KER}}, \tag{4b}$$

where m_{NO} and m_{15} are the masses of NO and the assumed identical O and N fragments, respectively; M is the total mass; and E_{NO}, E_2, and E_1 are the kinetic energies of the NO and the identical O and N particles of mass 15, respectively. The strengths of the Dalitz plot are the following. The plot is uniform when the momenta of the particles are fully uncorrelated only obeying momentum conservation. Further, each position in the plot reflects a specific asymptotic dissociation geometry (see Fig. 2 in Ref. 31). Figure 8 presents two Dalitz plots. Figure 8(a) reflects the parametrized dissociation events. Clearly, a very small part of the allowed area is oc-

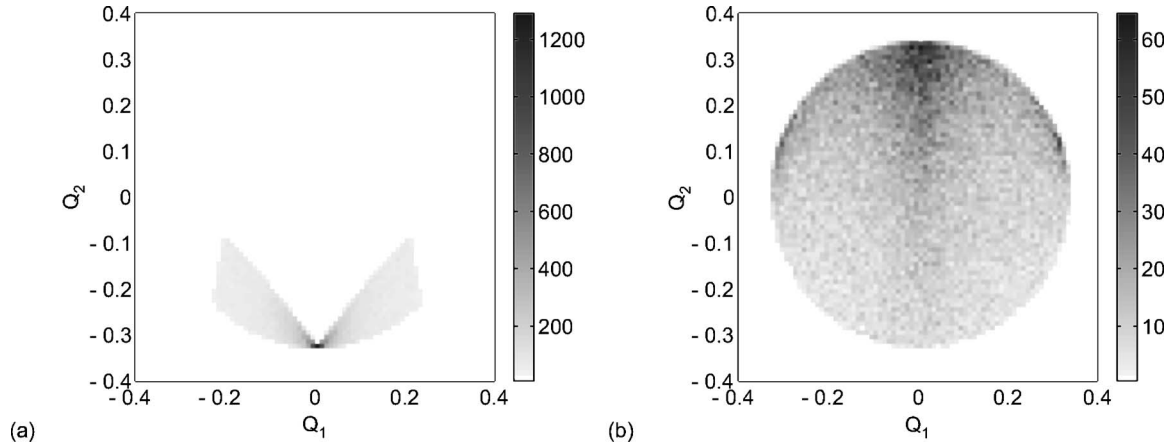

FIG. 8. Dalitz plots for a fixed total energy E in the DR of $(NO)_2^+$. For all events, Q_1 and Q_2 as shown in Eqs. (4a) and (4b) are calculated. Conservation of momentum restricts all events to a circle. For $Q_1=0$ and $Q_2=-0.4$ the events describe linear dissociation, O–NO–N. For $Q_1=0$ and $Q_2=+0.4$ the events describe dissociation in which the O and N fragments recoil in the same direction. In the case of uncorrelated dynamics or flat phase space, the resulting plot is flat, whereas correlation results in structure in the plot. (a) The Dalitz plot associated with the simulation shown in Fig. 6. A fixed KER value was chosen, since the dissociation dynamics for all internal energies of the NO fragment proved to be similar. The plot reveals significant correlation. (b) The Dalitz plot associated with the parametrization in which the χ and ρ distributions are random and uncorrelated. This is close, but not equal, to completely uncorrelated dynamics.

cupied pointing at highly correlated dissociation dynamics with an enhanced probability of linear dissociation leaving the NO fragments little kinetic energy. It is of interest to note that the parameters chosen to parametrize the dissociation dynamics, χ and ρ, do not generate a flat Dalitz plot when chosen randomly and uncorrelated. Figure 8(b) contains parameter plots in the case of random numbers for the two parameters. Although much more flat than found in our experiment, the resulting plot still reveals a nonflat phase space. The enhancement of probability at near-zero dissociation angles is a consequence of our choice to parametrize the angle of the light fragments with respect to the c.m. The second question is whether the measured data set excludes other parametrizations of the dissociation dynamics. Although a quantitative answer to this question is difficult, already removing the correlation between the parameters in a simulation reduces the agreement with the different parameter plots shown in Figs. 5 and 6. Nature is benignant in this case as the high degree of correlation with in general a small fraction of the energy going to the NO fragment facilitates the correct interpretation of the observed events.

The simulations provide the product-state distribution of NO(v), since the energies needed to excite the light fragments, O and N, are much larger. We have estimated the error in the branching fractions from simulations with varying distributions of χ and ρ that still describe the measured data reasonably well. The obtained product-state distribution shown in Fig. 9 is the mean internal-state density determined from each fit to the TD distribution with the error being the standard deviation. Contrary to the above analysis, the total kinetic energy in these simulations was set to decrease in steps of roughly two vibrational quanta (500 meV). The smaller ($\Delta v=1$) step gave rise to some erratic changes in the neighboring state contributions, while the larger bin turned out to be quite stable. Figure 9 shows that the NO($v=0$) limit is dominant. Additionally shown is the Franck-Condon overlap that we determined between the NO moiety of a NO dimer ion and a free NO. These Franck-Condon factors are scaled to the simulated NO($v=0$) product-state fraction and take the summation over adjacent vibrational levels into account. The Franck-Condon overlap predicts the minimum changes that are expected when a passive NO fragment goes from a bound NO moiety to a free NO in a sudden process. Although this figure shows discrepancies, the model may be correct still. We note that the total fragment internal energy, vibration plus rotation in the simulation, is compared to the vibrational energy spacing via the Franck-Condon factors. If a fraction of the excess energy ends up in rotational energy, the product vibrational distribution would agree more with the Franck-Condon factor prediction.

Finally, we want to point out a few minor points. In Fig.

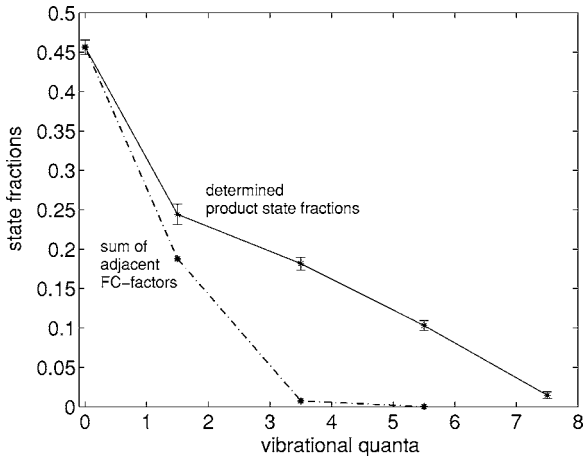

FIG. 9. The internal-energy distribution as follows from simulations with slightly differing parameter sets of χ and ρ and with internal-energy increments of 500 meV, equivalent to two vibrational quanta (solid curve). The production of $v=0$ and $v=1+2$ shows resemblance with the Franck-Condon overlap between the NO moiety in a $(NO)_2^+$ ion and a free NO, which accounts for the addition of two adjacent vibrational levels (dashed curve). The values used were $\omega_e(NO)=1904\ cm^{-1}$, $r_e(NO)=1.15$ Å for the free NO (Ref. 36) and $\omega_e(NO^{1/2+})=2110\ cm^{-1}$, $r_e(NO^{1/2+})=1.11$ Å for the NO moiety of the NO dimer ion (see Ref. 10).

6(a), there is a small signal at TD values above 22 mm, which is too high to be accounted for by a KER of 2.17 eV. The analysis of these events yields random dissociation dynamics without much correlation. This signal might be due to the small contribution of N_2+O+O fragmentation, which can have a much higher KER, or to false three-body events. The O_2+N+N fragmentation channel can only contribute to TD values of around 13 mm or lower. Furthermore, a small bump near TD values of 4–5 mm (arrow) is located around the position where the physical branching channel, $NO+N+O^*(^1D)$, is to be expected if present. The same events give the extra signal in the measured d_s distances indicated with an arrow [Fig. 6(b)] that cannot be accounted for by the simulation when assuming similar dynamics as for the other branching channels.

IV. DISCUSSION

We have studied the energy-dependent cross section, the chemical fragmentation pathways, and the fragmentation dynamics of the NO-dimer cation. Two scientific questions interested us prior to the experiment. The first interest was to look into the surprisingly large thermal rates observed in weakly bound dimer ions.[4,6] The second interest was to find out whether the dissociation of the dimer ion could be approximated as the DR of $NO.NO^+$, where the NO^+ would dissociate and the NO moiety would act as a spectator.

The thermal rate coefficients of dimer ions are surprisingly high. The $(NO)_2^+$ thermal rate coefficient determined from our data is around 1.5×10^{-6} cm^{-3}, in agreement with the thermal rate of 1.7×10^{-6} cm^{-3} determined by Weller and Biondi.[33] This rate is roughly a factor of 4 higher than that of the monomer, which is about 4×10^{-7} cm^{-3} at 300 K.[26] The thermal rates of O_2^+ and $O_2.O_2^+$ even differ with a factor of 20.[4] The high efficiency of the DR reaction in dimer ions is referred to as super-DR. A mechanism for this super-DR proposed by Bates[5,6] points at the consequence of potential-energy curves that cross with relatively small slopes. This increases the Franck-Condon overlap locally but not necessarily at low collision energy only. Our measurement gives a cross-section dependence of $\sigma_{DR}\sim E_c^{-1.4}$, which is steeper than for the monomer ion. As a consequence, the cross section of the dimer becomes comparable to that of the monomer already at 0.2 eV. A strong energy dependence is also observed in the DR of the proton-bridged $D_5O_2^+$ cluster ion.[34] Comparing the latter cross section to that of the DR of H_2O^+ reported by Jensen *et al.*[35] reveals a similar behavior; the cross sections are similar at 0.2 eV, while near 0 eV they differ by a factor of 10. As far as we know, no cross sections of other weakly bound dimer ions have been measured as a function of collision energy. The present observations may point at the importance of a high density of low-energy rovibrational states in the recombining system, promoting the capture efficiency or slowing the autoionization of the intermediate excited $(NO)_2^*$. Also, as Bates remarked, the DR of weakly bound dimer ions allows formation of Rydberg state fragments at low-energy electron collisions.[5] If this mechanism would be responsible for the high DR rates, then the dimer bond has to be very important in the DR reaction. Also in this case it is not clear why the high DR rate is restricted to the first 200 meV.

The chemical fragmentation study gave the interesting result that only two channels were represented (apart from a very small contribution of a third channel), while there are in total seven fragmentation channels energetically possible. The three-body channel $NO+O+N$ is dominant with a branching fraction of 69%. The next dominant channel is the two-body channel $NO+NO$ with a branching fraction of 23%. The dominance of the three-body channel is consistent with the studies on the DR of other polyatomic ions, in which the dominant fragmentation often is the three-body breakup. However, there is an important difference. In systems with equivalent covalent bonds and lighter atoms as in XH_2, the DR process seems to be nearly a statistical process. Indications for this exist both in the chemical fragmentation in the ratios, $X+H_2$ vs $XH+H$, and in the three-body dissociation dynamics. It was concluded that the DR generates doubly excited states that are repulsive in more than one coordinate.[28,29] In these systems, it has been shown that strong repulsive forces are accompanied by large torques that allow for considerable rearrangements. In the present system, the three-body dissociations may well be a consequence of repulsion in one coordinate (N…O) with the weak dimer bond unable to bind both atomic fragments. In this system, the special situation exists that the dominant channel for the monomer forming $O(^3P)+N^*(^2D)$ is energetically closed for the dimer ion. If the system depends on a repulsive curve leading to this channel, it finds itself a bound system, which will undoubtedly affect the final outcome. Due to the low signal-to-noise ratio, we have not been able to study the chemical branching nor the dissociation dynamics of $(NO)_2^+$ near 0.21 eV, which is the energy required to dissociate towards $O(^3P)+N^*(^2D)$. If this channel would also be dominant, the three-body branching may even further increase at this energy.

The dynamics of the three-body breakup into $NO+O+N$ reveals that the NO fragment can largely be considered as a passive spectator in the DR process. The vibrational ground state of the NO fragment is dominant and accounts for at least 45% of the dissociations, depending on the fraction of rotational energy imparted in the NO. Channels leading to internal excitation of the NO up to two vibrational quanta account for 69%. We find that the internal energy of the NO has little influence on the dissociation dynamics. However, the NO fragment is not fully passive as the energy partitioning over the O and N product atoms is correlated to the fragment dissociation angle. As the NO fragment receives less kinetic energy, the linear momentum between the O and N atoms is increasingly obeyed and the $(NO)_2^+$ dissociates increasingly as a linear system with angles close to 180°. In view of the present research on $(NO)_2^+$, it would be of interest to study the DR of O_4^+ for several reasons; it is a weakly bound system directly comparable to $(NO)_2^+$, the analysis and identification is simplified due to equal fragments and masses in the fragmentation and the possible

three-body dissociations, the dynamics of the monomer have been intensely investigated, the dominant physical branching channels of the monomer are also allowed for the dimer ion, and it has direct atmospheric relevance. A previous storage-ring experiment on O_4^+ failed due to insufficient current production.

V. CONCLUSIONS

The DR cross section of the $(NO)_2^+$ is an order of magnitude higher than its monomer counterpart at low energies. Nonetheless this cross section drops more steeply upon increasing collision energy than that of the monomer, resulting in comparable rates above 0.2 eV. This has large implications on the validity of the super-DR theorem suggested by Bates for dimer ions.[5,6] $(NO)_2^+$ breaks up mainly into two channels, the NO+O+N (69%) and the NO+NO (23%) channel. The three-body breakup is dominant, as is seen in the DR of many polyatomic ions. The DR of $(NO)_2^+$ into NO+O+N certainly has characteristics of a mechanism in which the recoil in the DR process is along one of the NO bonds. This forms the first detailed study into the DR mechanisms operating in weakly bound clusters. It is important to gather data on other systems in order to distinguish trends. Experimentally, we approach the limit of what is possible with the presently used imaging technology. Further detector development that combine high detection efficiency with fragment identification would give real progress.

ACKNOWLEDGMENTS

This work is part of the research program of the "Stichting voor Fundamenteel Onderzoek der Materie (FOM)," which is financially supported by the "Nederlandse Organisatie voor Wetenschappelijk Onderzoek (NWO)." Support has also been given by the EU research-training network Electron Transfer Reactions (ETR) under HPRN-CT-2000-00142 and by the Swedish Research Council. We are grateful to the staff members of the Manne Siegbahn Laboratory for their support during the experiments.

[1] J. L. Fox, J. Geophys. Res. **102**, 24005 (1997).
[2] R. R. Hodges, Jr., J. Geophys. Res. **105**, 6971 (2000).
[3] R. P. Wayne, *Chemistry of Atmospheres*, 3rd ed. (Oxford University Press, Oxford, 2000).
[4] J. B. A. Mitchell and C. Rebrion-Rowe, Int. Rev. Phys. Chem. **16**, 201 (1997).
[5] D. R. Bates, J. Phys. B **25**, 3067 (1992).
[6] D. R. Bates, J. Phys. B **24**, 703 (1991).
[7] L. Andrews and M. Zhou, J. Chem. Phys. **111**, 6036 (1999).
[8] C. L. Lugez, W. E. Thompson, M. E. Jacox, A. S. Snis, and I. Panas, J. Chem. Phys. **110**, 10345 (1999).
[9] B. Urban, A. Strobel, and V. E. Bondybey, J. Chem. Phys. **111**, 8939 (1999).
[10] Y. Xie and H. F. Schaeffer III, Mol. Phys. **98**, 955 (2000).
[11] Y. Xie, H. F. Schaeffer III, X.-Y. Fu, and R.-Z. Liu, J. Chem. Phys. **111**, 2532 (1999).
[12] Y. Xie, W. Wang, K. Fan, and H. F. Schaeffer III, J. Chem. Phys. **117**, 9727 (2002).
[13] I. Fischer, A. Strobel, J. Staecker, and G. Niedner-Schatteburg, J. Chem. Phys. **96**, 7171 (1992).
[14] S. H. Linn, Y. Ono, and C. Y. Ng, J. Chem. Phys. **74**, 3342 (1981).
[15] C. Y. Ng, P. W. Tiedemans, B. H. Mahan, and Y. T. Lee, J. Chem. Phys. **66**, 3985 (1977).
[16] F. Hellberg, A. Petrignani, W. J. van der Zande, S. Rosén, R. D. Thomas, A. Neau, and M. Larsson, J. Chem. Phys. **118**, 6250 (2003).
[17] A. Neau *et al.*, J. Chem. Phys. **113**, 1762 (2000).
[18] L. Vikor, A. Al-Khalili, H. Danared, N. Djuric, G. H. Dunn, M. Larsson, A. Le Padellec, S. Rosén, and M. af Ugglas, Astron. Astrophys. **344**, 1027 (1999).
[19] J. R. Peterson *et al.*, J. Chem. Phys. **108**, 1978 (1998).
[20] A. L. Padellec *et al.*, Phys. Rev. A **64**, 012702 (2001).
[21] A. Petrignani, P. C. Cosby, F. Hellberg, R. D. Thomas, M. Larsson, and W. J. van der Zande, J. Chem. Phys. **122**, 014302 (2005).
[22] M. B. Någård *et al.*, J. Chem. Phys. **117**, 5264 (2002).
[23] A. Al-Khalili *et al.*, Phys. Rev. A **68**, 042702 (2003).
[24] R. Peverall *et al.*, J. Chem. Phys. **114**, 6679 (2001).
[25] S. Datz, R. D. Thomas, M. Larsson, A. M. Derkatch, F. Hellberg, and W. J. van der Zande, Phys. Rev. Lett. **85**, 5555 (2000).
[26] L. Vejby-Christensen, D. Kella, H. D. Pedersen, and L. H. Andersen, Phys. Rev. A **57**, 3627 (1998).
[27] It is noted that other papers do not always include the $\sqrt{2}$ factor in the expression of the total displacement.
[28] R. Thomas, S. Rosén, F. Hellberg, A. M. Derkatch, M. Larsson, S. Datz, R. Dixon, and W. J. van der Zande, Phys. Rev. A **66**, 032715 (2002).
[29] R. D. Thomas, F. Hellberg, A. Neau, S. Rosén, M. Larsson, C. R. Vane, M. E. Bannister, S. Datz, A. Petrignani, and W. J. van der Zande, Phys. Rev. A **71**, 032711 (2005).
[30] R. H. Dalitz, Philos. Mag. **44**, 1068 (1953).
[31] D. Strasser, L. Lammich, H. Kreckel, M. Lange, S. Krohn, D. Schwalm, A. Wolf, and D. Zajfman, Phys. Rev. A **69**, 064702 (2004).
[32] L. Lammich, H. Kreckel, S. Krohn, M. Lange, D. Schwalm, D. Strasser, A. Wolf, and D. Zaifman, Radiat. Phys. Chem. **68**, 175 (2003).
[33] C. S. Weller and M. A. Biondi, Phys. Rev. **172**, 198 (1968).
[34] M. B. Någård *et al.*, J. Chem. Phys. **117**, 5264 (2002).
[35] M. J. Jensen, R. C. Bilodeau, O. Heber, H. B. Pedersen, C. P. Safvan, X. Urbain, D. Zajfman, and L. H. Andersen, Phys. Rev. A **60**, 2970 (1999).
[36] S. G. Lias, in NIST Chemistry WebBook, NIST Standard Reference Database Number 69, edited by K. P. Huber and G. Herzberg, data prepared by J. W. Gallagher and R. D. Johnson III (National Institute of Standards and Technology, Gaithersburg, MD, 2003); http://webbook.nist.gov